

Pressure-induced magnetic phase and structural transition in $SmSb_2$

Tao Li(李涛), Shuyang Wang(王舒阳), Xuliang Chen(陈绪亮), Chunhua Chen(陈春华), Yong Fang(房勇), Zhaorong Yang(杨昭荣)

Citation: Chin. Phys. B, 2024, 33 (**6**): 066401. DOI: 10.1088/1674-1056/ad362c
Journal homepage: http://cpb.iphy.ac.cn; http://iopscience.iop.org/cpb

What follows is a list of articles you may be interested in

Anomalous bond-length behaviors of solid halogens under pressure

Min Wu(吴旻), Ye-Feng Wu(吴烨峰), and Yi Ma(马毅)
Chin. Phys. B, 2021, 30 (**7**): 076401. DOI: 10.1088/1674-1056/abf4bd

Novel structures and mechanical properties of Zr_2N: *Ab initio* description under high pressures

Minru Wen(文敏儒), Xing Xie(谢兴), Zhixun Xie(谢植勋), Huafeng Dong(董华锋), Xin Zhang(张欣), Fugen Wu(吴福根), and Chong-Yu Wang(王崇愚)
Chin. Phys. B, 2021, 30 (**1**): 016403. DOI: 10.1088/1674-1056/abb220

A high-pressure study of Cr_3C_2 by XRD and DFT

Lun Xiong(熊伦), Qiang Li(李强), Cheng-Fu Yang(杨成福), Qing-Shuang Xie(谢清爽), Jun-Ran Zhang(张俊然)
Chin. Phys. B, 2020, 29 (**8**): 086401. DOI: 10.1088/1674-1056/ab8c3d

High pressure and high temperature induced polymerization of C_{60} quantum dots

Shi-Hao Ruan(阮世豪), Chun-Miao Han(韩春淼), Fu-Lu Li(李福禄), Bing Li(李冰), Bing-Bing Liu(刘冰冰)
Chin. Phys. B, 2020, 29 (**2**): 026402. DOI: 10.1088/1674-1056/ab6657

Structural transitions in $NaNH_2$ via recrystallization under high pressure

Yanping Huang(黄艳萍), Xiaoli Haung(黄晓丽), Xin Wang(王鑫), Wenting Zhang(张文亭), Di Zhou(周迪), Qiang Zhou(周强), Bingbing Liu(刘冰冰), Tian Cui(崔田)
Chin. Phys. B, 2019, 28 (**9**): 096402. DOI: 10.1088/1674-1056/ab37f8

Pressure-induced magnetic phase and structural transition in $SmSb_2$

Tao Li(李涛)[1,2], Shuyang Wang(王舒阳)[2,†], Xuliang Chen(陈绪亮)[1,2], Chunhua Chen(陈春华)[2], Yong Fang(房勇)[3], and Zhaorong Yang(杨昭荣)[1,2,4,5,‡]

[1] *Science Island Branch of Graduate School, University of Science and Technology of China, Hefei* 230026, *China*
[2] *Anhui Key Laboratory of Low-Energy Quantum Materials and Devices, High Magnetic Field Laboratory, HFIPS, Chinese Academy of Sciences, Hefei* 230031, *China*
[3] *Jiangsu Laboratory of Advanced Functional Materials, Department of Physics, Changshu Institute of Technology, Changshu* 215500, *China*
[4] *Institutes of Physical Science and Information Technology, Anhui University, Hefei* 230601, *China*
[5] *Collaborative Innovation Center of Advanced Microstructures, Nanjing* 210093, *China*

(Received 6 February 2024; revised manuscript received 19 March 2024; accepted manuscript online 21 March 2024)

Motivated by the recent discovery of unconventional superconductivity around a magnetic quantum critical point in pressurized $CeSb_2$, here we present a high-pressure study of an isostructural antiferromagnetic (AFM) $SmSb_2$ through electrical transport and synchrotron x-ray diffraction measurements. At $P_C \sim 2.5$ GPa, we found a pressure-induced magnetic phase transition accompanied by a $Cmca \rightarrow P4/nmm$ structural phase transition. In the pristine AFM phase below P_C, the AFM transition temperature of $SmSb_2$ is insensitive to pressure; in the emergent magnetic phase above P_C, however, the magnetic critical temperature increases rapidly with increasing pressure. In addition, at ambient pressure, the magnetoresistivity (MR) of $SmSb_2$ increases suddenly upon cooling below the AFM transition temperature and presents linear nonsaturating behavior under high field at 2 K. With increasing pressure above P_C, the MR behavior remains similar to that observed at ambient pressure, both in terms of temperature- and field-dependent MR. This leads us to argue an AFM-like state for $SmSb_2$ above P_C. Within the investigated pressure of up to 45.3 GPa and the temperature of down to 1.8 K, we found no signature of superconductivity in $SmSb_2$.

Keywords: high pressure, antiferromagnet, magnetoresistivity, structural transition

PACS: 64.70.k, 47.80.Fg, 61.50.Ks, 81.40.Vw **DOI:** 10.1088/1674-1056/ad362c

1. Introduction

Rare earth metals and intermetallics with 4f electrons have attracted great attention owing to rich exotic quantum phenomena they exhibited, such as heavy fermion state, quantum criticality, and unconventional superconductivity.[1–5] In these systems, many physical properties are governed by complex interplay between the underlying interactions, including strong Coulomb correlations, spin–orbit coupling (SOC), and the hybridization of the localized f electrons and conduction electrons. Recently, the addition nontrivial band topology in 4f electrons system open a new field in condensed-matter physics. For topological materials with 4f electrons, both SOC strength and spin texture play important role in the formation of nontrivial topology, which not only leads rich and unusual quantum phenomena[6–10] but also hold promise for application in electronic devices.[11–14]

The family of light rare-earth diantimonides $R Sb_2$ (R = La–Nd, Sm) displays combination of nontrivial band topology and electronic correlated effect, which crystallizes in layered orthorhombic structure with space group *Cmca*. It consists of alternatively stacked zigzag RSb bilayer and distorted square net of Sb layer along the c axis, as shown in Fig. 1(a), and we choose $SmSb_2$ as a representative. A charge density wave (CDW) order has been reported in $LaSb_2$ and $PrSb_2$,[15,16,18] and the former also displays superconductivity below $\sim$ 1 K.[19–22] All of $R Sb_2$ except $LaSb_2$ exhibit an antiferromagnetic (AFM) or a ferromagnetic ground state.[16,19,23–26] All $R Sb_2$ materials present large, linear and unsaturated magnetoresistivity (MR) with external magnetic field along c axis, while its origin still remains elusive.[19,23,27–30] Recently, the angle-resolved photo-emission spectroscopy measurement combined with first-principles calculations revealed non-trivial electronic topology in $LaSb_2$, and other isostructural $R Sb_2$ are also expected to have similar topological electronic bands.[30]

Pressure is an effective method to tune the lattice structure and to manipulate electronic states such as magnetism, superconductivity, and topological phases of matter without introducing impurities. By applying pressure to $LaSb_2$, the CDW state is suppressed, and the superconductivity shows dome-like diagram.[31,32] The recent discovery of unconventional superconductivity under pressure in ultraheavy fermion material $CeSb_2$ stimulated the re-research interest of the $R Sb_2$ family. The dome-type superconductivity appears near a magnetic quantum critical point, and its upper critical field exceeds the conventional Pauli limit eightfold.[33] Furthermore, high-pressure x-ray diffraction (XRD) measurements and calcula-

†Corresponding author. E-mail: sywang@hmfl.ac.cn
‡Corresponding author. E-mail: zryang@issp.ac.cn

© 2024 Chinese Physical Society and IOP Publishing Ltd

tions show that $LaSb_2$ and $CeSb_2$ exhibit a structural transition at 0.5 GPa and 1.7 GPa, respectively.[32,33] Therefore, it is highly interesting to investigate whether the emergence of the quantum critical point and novel states exist in other pressurized RSb_2 materials.

In this article, we choose $SmSb_2$ as an example, which present an AFM ordering at $T_N \sim 13.9$ K, and systematically study its high-pressure physical properties by utilizing electrical transports and synchrotron XRD in diamond anvil cells (DACs) with pressure up to 45.3 GPa. We find that the initial AFM state of $SmSb_2$ is insensitive to pressure below 2.5 GPa, above which another AFM-like phase shows up verified by our MR measurement. The transition temperature of the emergent AFM phase increase quickly with increasing pressure. The XRD measurements show that the magnetic phase transition is due to an orthorhombic *Cmca* to tetragonal *P*4/*nmm* structural phase transition.

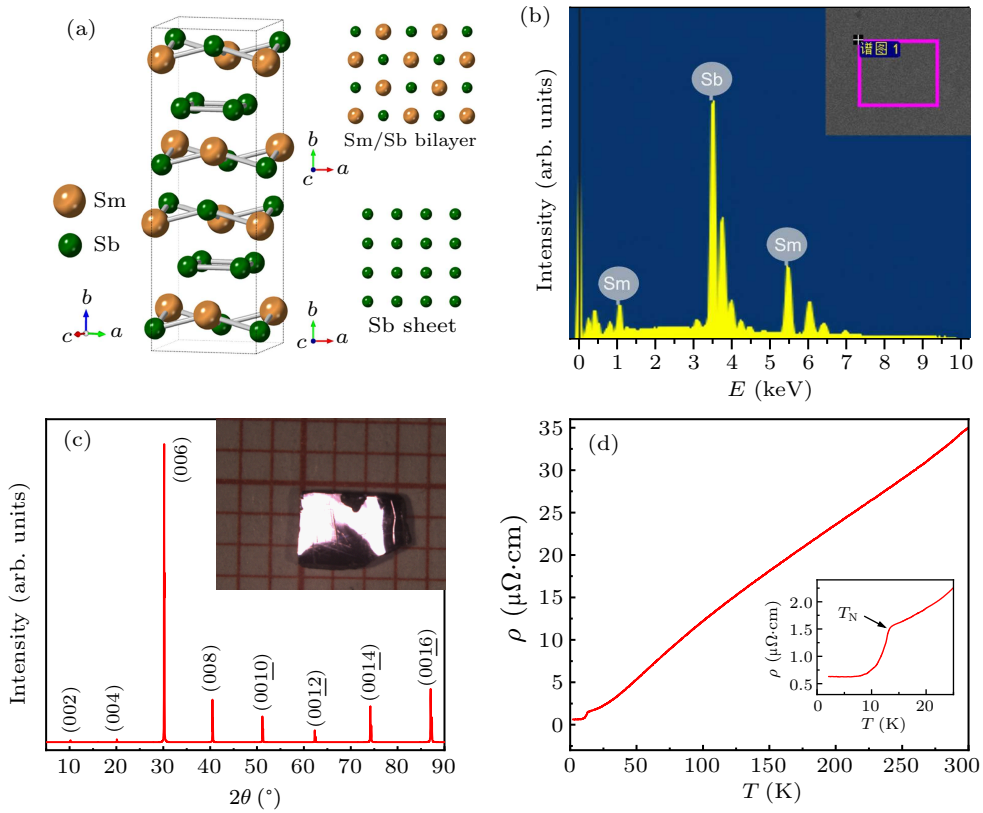


Fig. 1. (a) Crystal structure of $SmSb_2$. (b) Energy-dispersive x-ray spectroscopy. (c) Single crystal XRD pattern of $SmSb_2$. The inset presents a photo of one as-grown $SmSb_2$ single crystal. (d) Temperature dependence of resistivity at ambient pressure. The inset shows the blowup of the low-temperature resistivity.

2. Experimental methods

Single crystals of $SmSb_2$ were grown by the Sb-flux method, and the details of the crystal-growth procedure are given in Ref. [34]. The single crystal XRD pattern was collected by using an in-lab x-ray diffractometer with Cu $K\alpha$ radiation of wavelength 1.5406 Å at room temperature. The atomic ratio is analyzed by energy dispersive x-ray spectrometry (EDXS). Ambient-pressure electrical transport measurements were carried out in a physical property measurement system. High-pressure electrical transport measurements were performed in an in-house transport property measurement system using a nonmagnetic Be–Cu DAC.[35] The standard four-probe method was applied on single-crystal $SmSb_2$, and NaCl was used as the pressure-transmitting medium. The current was applied parallel to the *ab* plane, and the magnetic field was applied perpendicular to the *ab* plane. High pressure angle-dispersive synchrotron XRD ($\lambda = 0.6199$ Å) were performed on crushed $SmSb_2$ single crystals in a Mao–Bell cell with Daphne 7373 oil as pressure-transmitting medium at the beamline BL15U1 of Shanghai Synchrotron Radiation Facility. All above pressure values were calibrated with the ruby fluorescence shift at room temperature.[36] The Dioptas program was employed for the XRD image integrations.[37] The XRD patterns were fitted by using the RIETICA program with the Le Bail method.[38]

3. Results and discussion

We first characterized the ambient-pressure physical properties of $SmSb_2$, which demonstrated high quality of the single-crystalline samples. The EDXS spectrum gives an atomic ratio of Sm:Sb as 1:2.06, which is close to the ideal stoichiometry (see Fig. 1(b)). The single-crystal XRD pattern

only consists (00l) peaks, indicating that ab plane is natural cleavage facet of the crystals, as shown in Fig. 1(c). Figure 1(d) presents in-plane resistivity (ρ) as a function of temperature (T) at ambient pressure. The ρ–T curve shows a metallic-like behavior in the whole temperature range besides a sharp drop around $T_N = 13.9$ K (Fig. 1(d) inset) due to the antiferromagnetic transition, in agreement with the previous report.[19]

The temperature dependence of the in-plane resistivity from 0 GPa to 45.3 GPa are given in Fig. 2. Under pressures up to 1.1 GPa, the ρ–T curve shows similar behavior as that at ambient-pressure, in addition to small increment of T_N. At a critical pressure $P_C \sim 2.5$ GPa, another kink manifests around a higher temperature $T_N' \sim 17.5$ K and coexists with the initial one (14.6 K) in the ρ–T curve, as shown in Fig. 2(b). The newly appeared kink anomaly at T_N' can be associated with an AFM ordered state as discussed below. With further increasing pressure above 5.2 GPa, the original AFM kink disappears completely and T_N' keeps moving towards higher temperatures [see Fig. 2(c)], and the resistivity globally gets enhanced. Since this kink-type anomaly gradually broaden under high pressure, we define T_N' by cross point of two straight lines above and below the transition. Up to 45.3 GPa, the highest pressure in our measurement, T_N' reaches around 56 K.

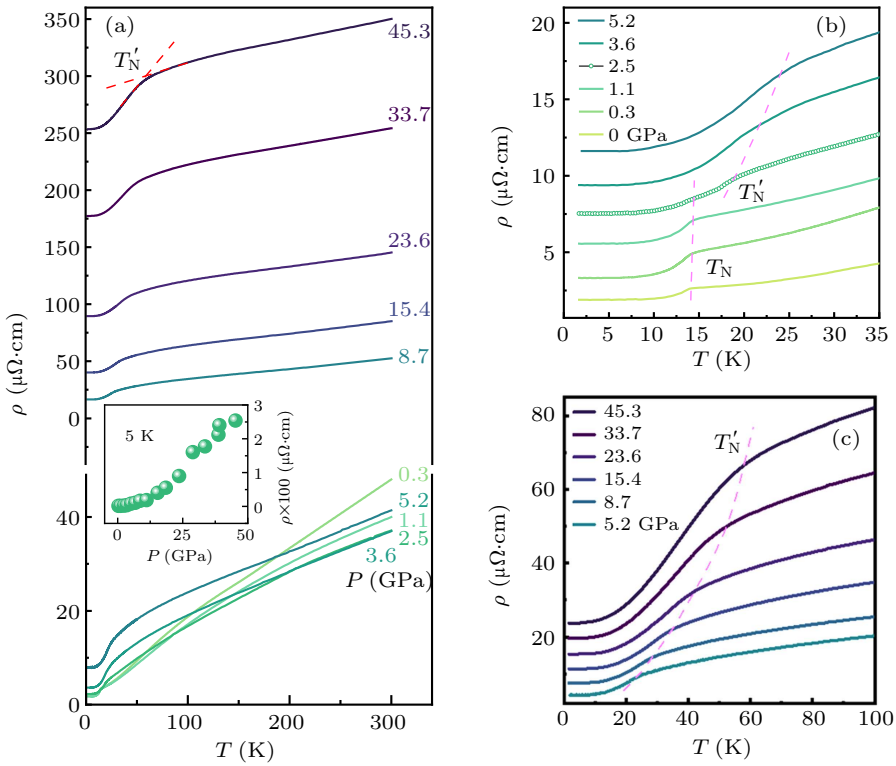


Fig. 2. (a) Temperature dependence of ρ at various pressures. The T_N' is defined as cross point of extended red dashed line through the data points. Inset shows the resistivity at 5 K at different pressures. (b)–(c) The enlarge view of low-temperature ρ and the data are shifted vertically for clarity. The pink dashed lines are guide to eyes highlighting the evolution of the T_N and T_N' evolution with pressures.

We then performed electrical transport measurements under external magnetic fields to investigate the origin of the anomaly in ρ–T curve. Figures 3(a) and 3(b) present the evolution of resistivity under different fields at ambient-pressure and 5.2 GPa respectively, and figures 3(c) and 3(d) present the corresponding temperature-dependent MR. Here, MR is defined as [MR $= (\rho(H) - \rho(0\ \mathrm{T}))/\rho(0\ \mathrm{T}) \times 100\%$], where $\rho(H)$ represents resistivity under a field and $\rho(0\ \mathrm{T})$ represents resistivity under zero field. At ambient pressure, T_N remains unaltered up to 8 T, suggesting that it is very hard to align the spins along the c axis. Moreover, the MR increases remarkably below T_N and saturates below 5 K. Interestingly, when we applied external magnetic field to $SmSb_2$ above P_C at 5.2 GPa, we find that the T_N' is still insensitive to the field and the MR increases significantly upon cooling below the T_N', which is similar as our ambient-pressure measurement. Singha *et al.*[19] suggested that the MR value strongly depends on carriers mobilities. As the temperature decreases, the carrier mobilities increase and suddenly enhance around the magnetic transition temperature due to the transition of magnetic moments from a disordered to an ordered state.[19]

We also measured MR at 2 K under various pressures as shown in Fig. 3(e). At ambient pressure, it can be observed that an unsaturated positive MR as large as $\sim 1200\%$ is obtained at 2 K and 8 T with almost linear under high field. With applying pressure, the magnitude of MR decreases dramatically from 390% at 0.3 GPa to 6% at 12.9 GPa. It is noticed that the MR at 2 K is keep positive above P_C, which is differ-

ent from typical negative MR of FM transition due to significant suppression of critical FM fluctuations near the ordering temperature.[39,40] The suppressed MR may attribute to reduction of the carrier mobility under pressure due to the presence of disorder in the sample.[39] The reduction of the carrier mobility under pressure is also reflected in the inset of Fig. 2(a), indicating that the resistivity at 5 K increases monotonically with pressures. For a pressure above P_C, the MR also shows positive value and presents linear field-dependent behavior with no sign of saturation up to 8 T, suggesting the unchanged MR mechanism across the magnetic transition. According to above MR measurement, we conclude that the emergent kink at T_N' on ρ–T curve above P_C origins from a magnetic transition, which could potentially remain an AFM order. In the future, $SmSb_2$ would particularly benefit from further clarification of the magnetic structures under pressures, by using magnetizations, neutron measurements, and theoretical calculations.

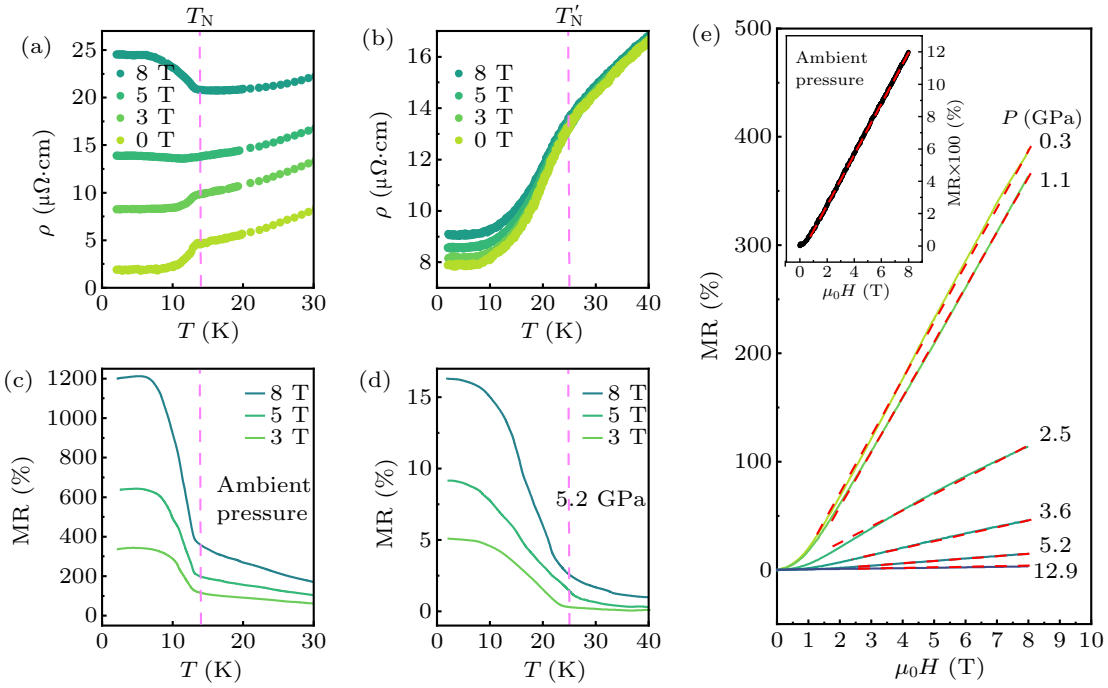


Fig. 3. (a) and (b) Temperature dependence of ρ under various fields at ambient pressure and 5.2 GPa, respectively. (c) and (d) Temperature-dependent MR at ambient pressure and 5.2 GPa, respectively. The pink dashed line denotes the temperature of the magnetic transition. (e) MR as a function of field at representative pressures and a fixed temperature of 2 K. The inset shows the MR at ambient pressure. The dashed red lines denote the linear behavior at various pressures.

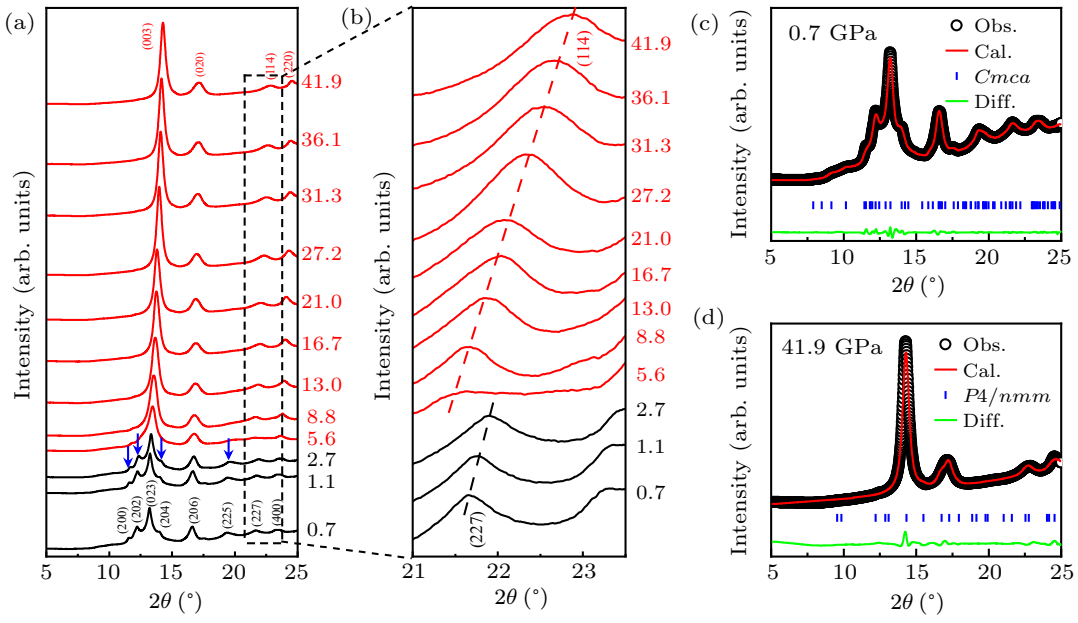


Fig. 4. (a) Room-temperature synchrotron XRD patterns of $SmSb_2$ at various pressures ($\lambda = 0.6199$ Å). The blue arrows present the disappeared peaks from initial *Cmca* structure. (b) Focused views of XRD peaks at around 22°, which highlight distinct downshift of peak under high pressure. The dashed lines are guides to eye, (c) and (d) representative fittings of the XRD patterns at 0.7 GPa and 41.9 GPa.

We then performed *in-situ* high-pressure synchrotron XRD experiments on $SmSb_2$ to investigate the relationship between magnetism and structural modulation. The XRD patterns up to 41.9 GPa are presented in Fig. 4(a). From 0.7 GPa to 2.7 GPa, all XRD peaks move towards higher angles monotonically due to shrinkage of the $SmSb_2$ lattice, and the XRD patterns can be fitted by the initial phase with space group *Cmca*. Starting from 5.6 GPa, some diffraction peaks, such as (200), (202), (204), and (225) peaks, from the original *Cmca* structure disappear (as indicated by blue arrows), and some peaks show distinct downshift, as exhibited in Fig. 4(b) as an example. These observations indicate structural phase transition from low symmetry to high symmetry between 2.7 GPa–5.6 GPa, in line with the magnetic transition from the above transport result. Above 5.6 GPa, the XRD peaks move towards higher angles with increasing pressure and remaining up to the highest pressure of 41.9 GPa, suggesting completion of the structural transition.

Recent studies suggested that isostructural $LaSb_2$ and $CeSb_2$ shifts structurally from *Cmca* to *Cmcm* under pressures.[32,33] However, the fitting is failed to $SmSb_2$ by using the *Cmcm* phase above 5.6 GPa, suggesting that $SmSb_2$ may not adopt the *Cmcm* phase at high pressures. Considering the feasible phase for the high-pressure structure in $SmSb_2$, we then focused on the discovered structures in AB_2 family (*A* is rare earth or actinide elements; *B* is other d or p-block metals), which crystallize in a series of crystal structure, including *Fd*-3*m*, *P*6/*mmm*, *P*4/*nmm*, and so on.[41] After careful analysis and fitting of data, we found that the XRD patterns above 5.6 GPa can be well fitted by tetragonal structure with space group *P*4/*nmm*. Two representative XRD pattern fitting results at 0.7 GPa and 41.9 GPa are presented in Figs. 4(c) and 4(d).

Figure 5(a) shows the pressure-induced structural transition from *Cmca* to *P*4/*nmm* corresponds to shift in *ab*-plane and a collapse of the *c* axis. The extracted lattice parameters and unit-cell volume of $SmSb_2$ under high pressure are exhibited in Figs. 4(b) and 4(c), respectively. The equation of state (EOS) was fitted by using the third-order Birch–Murnaghan formula[42]

$$P = \frac{3}{2}B_0[(V_0/V)^{7/3} - (V_0/V)^{5/3}] \times\left\{1+\frac{3}{4}(B_0'-4)[(V_0/V)^{2/3}-1]\right\}, \quad (1)$$

where V_0, B_0, and B_0' are the volume, bulk modulus $-V/(\mathrm{d}V/\mathrm{d}P)$, and first-order derivative of the bulk modulus at zero pressure, respectively. The fits yield $B_0 = 79.2 \pm 3.7$ GPa and $B_0' = 1.8 \pm 1.2$ for the *Cmca* phase and $B_0 = 119.8 \pm 5.5$ GPa and $B_0' = 9.6 \pm 4.3$ for the *P*4/*nmm* phase. The structural phase transition yields a unit-cell volume contraction $\Delta V/V \sim 8.4\%$ (Fig. 5(e)).

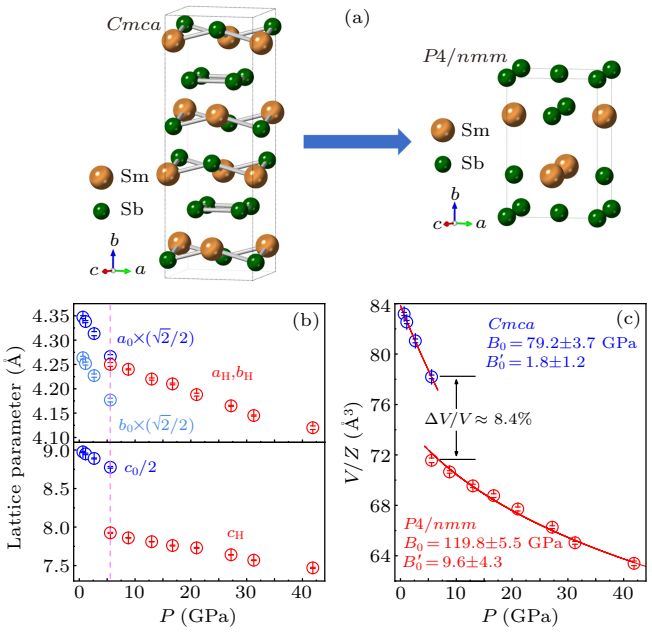


Fig. 5. (a) Schematics of the crystal structures of the pristine structure (*Cmca* phase) and the high-pressure structure (*P*4/*nmm* phase). (b) Pressure-dependent lattice parameters a_0, b_0, and c_0 of *Cmca* phase and a_H (b_H) and c_H of *P*4/*nmm*. (c) Unit cell volume per formula unit (V/Z) as a function of pressure. The solid lines are fits based on the third-order Birch–Murnaghan equation of state.

We conclude the above results into a phase diagram for $SmSb_2$ in Fig. 6. We observed that the T_N of $SmSb_2$ increases with increasing pressure with a rate of ~ 0.28 K/GPa, followed by a jump to T_N' accompanied by a structural transition from *Cmca* to *P*4/*nmm*. The T_N' initially increases rapidly with increasing pressure, while the increasing rate gradually slows down. Note that the phase diagram of $SmSb_2$ is quite different with that of the $CeSb_2$. In $CeSb_2$, the magnetic transition temperature is suppressed in high-pressure *Cmcm* phase, and the superconductivity emerge around the magnetic quantum critical point.[33] In the *P*4/*nmm* phase of $SmSb_2$, the AFM-like transition temperature is significantly enhanced to about 56 K at 45.3 GPa, which is quadruple the value observed in the *Cmca* phase. The AFM-like transition temperature of 56 K is also much higher than that of other RSb_2 material at ambient pressure,[19] indicating that the *P*4/*nmm* structure may play an important role in the establishment of magnetic order. The enhancement of T_N' in $SmSb_2$ is consistent with the Doniach phase diagram, which describes the behavior of T_N' as the result of competition between Ruderman–Kittel–Kasuya–Yosida (RKKY) and Kondo interactions.[43–45] When changing into the high pressure structure, $SmSb_2$ localizes in the far left part of the Doniach phase diagram dominated by RKKY interaction. In this region, the increase in hybridization strength primarily enhances the RKKY interaction under pressure, resulting in the promotion of magnetic order. With further compression, as supported by slow rate of T_N' increase, the Kondo spin would suppress the RKKY interaction, causing the magnetic ordering temperature to reach a maximum and then rapidly decrease towards the quantum critical point

at 0 K, similar to the observation in Nd metal, $PrTi_2Al_{20}$ and $CeRhIn_5$.[46–48] As a result, it may require significantly higher pressures to suppress the magnetic order in $SmSb_2$.

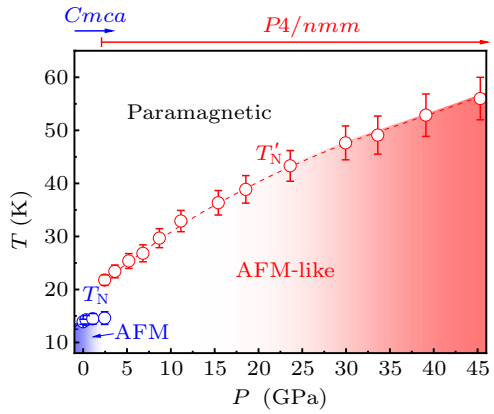


Fig. 6. Magnetic ordering temperature of $SmSb_2$ *versus* pressure. The dashed line through the data points is a guide to eye. The error bars give uncertainty in T_N and T'_N values.

4. Conclusion

In conclusion, we have systematically investigated the high-pressure properties of the AFM $SmSb_2$ by high-pressure electrical transports and XRD measurements with pressure up to 45.3 GPa. Our data show that the initial antiferromagnetic (AFM) order is maintained under applied pressures below $P_C \sim 2.5$ GPa. Beyond P_C, a new AFM-like state emerges, owing to a structural phase transition from an orthorhombic *Cmca* phase to a tetragonal *P4/nmm* phase. The transition temperature of the emergent magnetic phase keeps increasing in our pressure range. Further higher pressure may suppress the magnetic order and could induce superconductivity.

Acknowledgements

Project supported by the National Key Research and Development Program of China (Grant Nos. 2023YFA1406102 and 2022YFA1602603), the National Natural Science Foundation of China (Grant Nos. 12374049 and 12174395), the China Postdoctoral Science Foundation (Grant No. 2023M743542), Hefei Institutes of Physical Science, Chinese Academy of Sciences the Director's Fundation of (Grant No. YZJJ2024QN41), and the Basic Research Program of the Chinese Academy of Sciences Based on Major Scientific Infrastructures (Grant No. JZHKYPT-2021-08).

References

[1] Steglich F and Wirth S 2016 *Rep. Prog. Phys.* **79** 084502
[2] Scalapino D J 2012 *Rev. Mod. Phys.* **84** 1383
[3] Morosan E, Natelson D, Nevidomskyy A H and Si Q M 2012 *Adv. Mater.* **24** 4896
[4] Gegenwart P, Si Q and Steglich F 2008 *Nat. Phys.* **4** 186
[5] Stewart S G 1984 *Rev. Mod. Phys.* **56** 755
[6] Niu R and Zhu W 2021 *J. Phys.: Condens. Matter* **34** 113001
[7] Yin J X, Ma W, Cochran T A, Xu X, Zhang S S, Tien H J, Shumiya N, Cheng G, Jiang K and Lian B 2020 *Nature* **583** 533
[8] Tafti F, Gibson Q, Kushwaha S, Haldolaarachchige N and Cava R 2016 *Nat. Phys.* **12** 272
[9] Dzero M, Xia J, Galitski V and Coleman P 2016 *Annu. Rev. Condens. Matter Phys.* **7** 249
[10] Weng H, Yu R, Hu X, Dai X and Fang Z 2015 *Adv. Phys.* **64** 227
[11] Tokura Y, Yasuda K and Tsukazaki A 2019 *Nat. Rev. Phys.* **1** 126
[12] Tang F, Po H C, Vishwanath A and Wan X 2019 *Nature* **566** 486
[13] Šmejkal L, Mokrousov Y, Yan B and MacDonald A H 2018 *Nat. Phys.* **14** 242
[14] Bansil A, Lin H and Das T 2016 *Rev. Mod. Phys.* **88** 021004
[15] Luccas R F, Fente A, Hanko J, Correa-Orellana A, Herrera E, Climent-Pascual E, Azpeitia J, Pérez-Castañeda T, Osorio M and Salas-Colera E 2015 *Phys. Rev. B* **92** 235153
[16] Kagawa A, Kagayama T, Oomi G, Mitamura H, Goto T, Canfield P and Bud'ko S 2000 *Physica B: Condens. Matter* **281** 124
[17] Kawaguchi K, Kagayama T, Oomi G, Canfield P and Bud'Ko S 1997 *Physica B* **237** 587
[18] Palacio I, Obando-Guevara J, Chen L, Nair M, Barrio M G, Papalazarou E, Le Fèvre P, Taleb-Ibrahimi A, Michel E and Mascaraque A 2023 *Appl. Surf. Sci.* **610** 155477
[19] Bud'ko S L, Canfield P, Mielke C and Lacerda A 1998 *Phys. Rev. B* **57** 13624
[20] Fischer K F, Roth N and Iversen B B 2019 *J. Appl. Phys.* **125** 045110
[21] Galvis J, Suderow H, Vieira S, Bud'ko S and Canfield P 2013 *Phys. Rev. B* **87** 214504
[22] Guo S, Young D, Adams P, Wu X, Chan J Y, McCandless G and DiTusa J 2011 *Phys. Rev. B* **83** 174520
[23] Singha R, Yuan F, Lee S B, Villalpando G V, Cheng G, Singh B, Sarker S, Yao N, Burch K S and Schoop L M 2023 *Adv. Funct. Mater* **23** 2308733
[24] Trainer C, Abel C, Bud'ko S L, Canfield P C and Wahl P 2021 *Phys. Rev. B* **104** 205134
[25] Liu B, Wang L, Radelytskyi I, Zhang Y, Meven M, Deng H, Zhu F, Su Y, Zhu X and Tan S 2020 *J. Phys.: Condens. Matter* **32** 405605
[26] Zhang Y, Zhu X, Hu B, Tan S, Xie D, Feng W, Qin L, Zhang W, Liu Y, Song H, Luo L, Zhang Z and Lai X 2017 *Chin. Phys. B* **26** 067102
[27] Ruszała P, Winiarski M and Samsel-Czekała M 2020 *Acta Phys. Pol. A* **138** 748
[28] Young D, Goodrich R, DiTusa J, Guo S, Adams P, Chan J Y and Hall D 2003 *Appl. Phys. Lett.* **82** 3713
[29] Goodrich R, Browne D, Kurtz R, Young D, DiTusa J, Adams P and Hall D 2004 *Phys. Rev. B* **69** 125114
[30] Qiao Y, Tao Z, Wang F, Wang H, Jiang Z, Liu Z, Cho S, Zhang F, Meng Q and Xia W 2022 arXiv:2208.10437 [cond-mat.str-el]
[31] Bud'ko S L, Huyan S, Herrera-Siklody P and Canfield P C 2023 *Philos. Mag.* **103** 561
[32] Weinberger T I, de Podesta C K, Chen J, Hodgson S A and Grosche F M 2023 *SciPost Phys.* **11** 018
[33] Squire O P, Hodgson S A, Chen J, Fedoseev V, de Podesta C K, Weinberger T I, Alireza P L and Grosche F M 2023 *Phys. Rev. Lett.* **131** 026001
[34] Canfield P C, Thompson J D and Fisk Z 1991 *J. Appl. Phys.* **70** 5992
[35] Zhou Y, Chen X, An C, Zhou Y, Ling L, Yang J, Chen C, Zhang L, Tian M, Zhang Z and Yang Z 2019 *Phys. Rev. B* **99** 054501
[36] Mao H, Xu J A and Bell P 1986 *J. Geophys. Res. Solid Earth* **91** 4673
[37] Prescher C and Prakapenka V B 2015 *High. Press. Res.* **35** 223
[38] Hunter B 1998 *Newsletter* **20**
[39] Zhou Y, Chen X, Zhou Y, Yu J, Zhu X, An C, Park C, Wan X, Yang X and Yang Z 2022 *Sci. China. Phys. Mech.* **65** 288211
[40] Geishendorf K, Schlitz R, Vir P, Shekhar C, Felser C, Nielsch K, Goennenwein S T and Thomas A 2019 *Appl. Phys. Lett.* **114** 092403
[41] Chandra Shekar N V, Sahu P C, Sanjay Kumar N R, Sekar M, Subramanian N, Kathirvel V, Chandra S and Rajagopalan M 2009 *Solid State Phenom.* **150** 123
[42] Birch F 1947 *Phys. Rev.* **71** 809
[43] Yang Y F, Fisk Z, Lee H O, Thompson J and Pines D 2008 *Nature* **454** 611
[44] Iglesias J R, Lacroix C and Coqblin B 1997 *Phys. Rev. B* **56** 11820
[45] Doniach S 1977 *Physica B* **91** 231
[46] Song J, Bi W, Haskel D and Schilling J 2017 *Phys. Rev. B* **95** 205138
[47] Matsubayashi K, Tanaka T, Sakai A, Nakatsuji S, Kubo Y and Uwatoko Y 2012 *Phys. Rev. Lett.* **109** 187004
[48] Hegger H, Petrovic C, Moshopoulou E, Hundley M, Sarrao J, Fisk Z and Thompson J 2000 *Phys. Rev. Lett.* **84** 4986